

SURFACE MORPHOLOGY AND HARDNESS OF POWDER BED FUSED SS316L AS A FUNCTION OF PROCESS PARAMETERS

S.H. Jagdale, S. Theeda, B. B. Ravichander, G. Kumar

Department of Mechanical Engineering, The University of Texas at Dallas, Richardson, TX
75080.

Abstract

Laser powder bed fusion is an emerging additive manufacturing process to fabricate fully dense complex metal parts with high accuracy. Laser process parameters such as, laser power, hatch spacing, scan speed, scan strategy and layer thickness play a major role in defining the quality of the as-built parts. Stainless steel 316L (SS316L) is known for its excellent corrosion resistance, high tensile strength, and high-performance at elevated temperatures. SS316L is used in many applications in the field of automotive, aerospace, medical and heavy equipment industries. In the current study, experiments are designed using Taguchi method to understand the effect of process parameters on the mechanical properties of as-built SS316L parts. Surface roughness of as-built parts is characterized by using digital optical microscopy. The relative density and Vickers microhardness are measured for the as-built parts. Finally, an optimal processing region for laser process parameters is identified.

Keywords: Laser Powder Bed Fusion, SS316L, Microhardness, Design of Experiments, Taguchi, Surface Roughness

1. INTRODUCTION

Stainless Steel 316L (SS316L) exhibits excellent corrosion resistance and mechanical properties [1]. The presence of Chromium in SS316L improves the corrosion resistance [2] and makes it suitable for applications in biomedical, marine, petroleum and food industry. Other properties such as, mechanical strength, fracture toughness and machinability can be improved with the addition of elements like Nickel, Molybdenum and Nitrogen [2]. Due to the combination of these properties, SS316L is widely used as a structural material [3, 4]. Better performance of the product demands complex and innovative part designs but the manufacturing capability of conventional processes like casting, forming and machining is limited and cannot fulfill the design requirements [5].

Laser Powder Bed Fusion (LPBF) is one of the metal 3D printing methods which allows an unmatched flexibility in designing of complex parts from metal powders. A thin layer of metal powder is spread by recoater on a metal substrate [6, 7], which is then scanned with high intensity laser to fuse the powder particles together by melting and solidification. Subsequently, another layer of powder is spread and scanned, and the process is repeated until the part is completely fabricated [6, 8-10]. LPBF is typically carried out under inert atmosphere (Argon, Nitrogen or Helium). Parts fabricated with LPBF are highly dense and exhibit properties comparable to the cast and machined counterparts. Laser power, scan speed, scan strategy, hatch spacing and layer thickness are major processing parameters which affect the properties of parts fabricated by LPBF.

These process parameters lead to variation in the microstructure and mechanical properties [11, 12]. Use of LPBF machines from different manufacturers can also result in different properties of parts produced with the same process parameters [13]. Therefore, it is important to systematically vary the process parameters using the same machine in a specific material to unravel the underlying mechanism in metal 3D printing.

Tucho *et al.* investigated the effect of process parameters such as, scan speed, hatch spacing and laser power on the hardness and relative density of Selective Laser Melted (SLM) SS316L parts [14]. It was observed that parts fabricated with large hatch spacing showed lower relative density [14]. Similar study of understanding the effect of process parameters on the hardness and roughness of SLM SS316L was conducted by Cherry *et al.* [15]. Laohaprapanon *et al.* used 2^k factorial design to study the effect of laser power, scan speed and hatch spacing on the relative density and microhardness of SLM SS316L parts [16]. Only few experiments with extreme range of process parameters were selected in the previous study [16]. Increase in relative density was observed with increasing energy density [16]. Taguchi's L16 orthogonal array-based design of experiments (DOE) was used by Aqilah *et al.* to understand the influence of laser power, hatch spacing and scanning speed on the surface roughness of SLM SS316L [17]. It was found that the laser power is the most influential factor compared to the hatch spacing and the scanning speed in LPBF process [17]. Koziar *et al.* evaluated the influence of build orientation on the surface properties of LPBF SS316L in order to address the challenge of surface texture quality and printing resolution in the design and 3D printing of microelectromechanical systems (MEMS) models [18]. Greco *et al.* studied the impact of laser power, layer thickness and hatch spacing on the roughness, density and microhardness of SLM AISI316L by keeping constant input energy density [19]. In their study, it was noted that parts fabricated with constant energy density but with varying process parameters had different properties [19]. Khorasani *et al.* studied the effect of laser process parameters on the density, hardness, and surface quality of Ti-6Al-4V [20]. The experiments were designed based on the Taguchi L25 orthogonal array [20]. In another study, Ravichander *et al.* used response surface methodology-based design of experiment to analyze the effect of LPBF process parameters on the hardness of as-built IN718 parts [21].

Although several studies have been done on understanding the effect of LPBF process parameters on the properties of SS316L, very few have considered the effect of scan strategy. Also, lots of studies were carried out without designing the experiments systematically. Therefore, in this work, comprehensive study of effect of LPBF process parameters such as scan strategy, laser power, hatch spacing and scan speed on the surface roughness and microhardness of SS316L is carried out. Experiments are designed based on Taguchi's mixed level design. Cubical specimens are fabricated with SLM solutions 125HL SLM machine.

2. Materials and Methods

2.1 Design of Experiments

Minitab V21 (Minitab Inc., State College, PA, USA) was utilized to establish the mixed level Taguchi's design. The Taguchi's robust design of experiment is used to optimize numerous process parameters simultaneously and to extract quantitative information from fewer experimental trials. The experimental design consisted of laser power, scan speed, hatch spacing and scan strategy as the control parameters listed in Table 1. The layer thickness was kept at 30 μm for all the samples to ensure consistency. Thus, based on the obtained design, a total of 32 parameter set was obtained (Table 2). The samples were characterized by Vickers hardness and

surface roughness measurements. Further, 2D contour plots were plotted along with main effects plot to analyze the influence of each process parameter set on the desired outputs. It is also worth mentioning that different values for process parameter sets resulted in different energy density values which was calculated using following formula [12, 21-23]:

$$E_v = \frac{LP}{SS \times HS \times LT}$$

where E_v (J/mm^3) is the energy density, LP (W) is the laser power, SS (mm/s) is the scanning speed, HS (μm) is the hatch spacing, and LT (μm) is the layer thickness.

Table 1: Selected process parameters for DOE and their levels

Process Parameter (Factors)	Level 1	Level 2	Level 3	Level 4
Scan Strategy	Stripes	Chess	-	-
Laser Power (W)	150	185	220	255
Scan Speed (mm/s)	710	770	830	890
Hatch Spacing (μm)	111	117	123	129

Table 2: Complete DOE based on Taguchi's mixed level design

Sample No.	Scan Strategy	Laser Power (W)	Scan Speed (mm/s)	Hatch Spacing (μm)	Energy Density (J/mm^3)
1	Stripes	150	710	111	63.44
2	Stripes	150	770	117	55.50
3	Stripes	150	830	123	48.98
4	Stripes	150	890	129	43.55
5	Stripes	185	710	111	78.25
6	Stripes	185	770	117	68.45
7	Stripes	185	830	123	60.40
8	Stripes	185	890	129	53.71
9	Stripes	220	710	117	88.28
10	Stripes	220	770	111	85.80
11	Stripes	220	830	129	68.49
12	Stripes	220	890	123	66.99
13	Stripes	255	710	117	102.32
14	Stripes	255	770	111	99.45
15	Stripes	255	830	129	79.39
16	Stripes	255	890	123	77.65
17	Chess	150	710	129	54.59
18	Chess	150	770	123	52.79

19	Chess	150	830	117	51.49
20	Chess	150	890	111	50.61
21	Chess	185	710	129	67.33
22	Chess	185	770	123	65.11
23	Chess	185	830	117	63.50
24	Chess	185	890	111	62.42
25	Chess	220	710	123	83.97
26	Chess	220	770	129	73.83
27	Chess	220	830	111	79.60
28	Chess	220	890	117	70.42
29	Chess	255	710	123	97.33
30	Chess	255	770	129	85.57
31	Chess	255	830	111	92.26
32	Chess	255	890	117	81.63

2.2 Powder Preparation and Fabrication

A total of 32 cubical SS 316L specimens of dimensions 8mm x 8mm x 6mm were fabricated using LPBF printer SLM 125 HL (SLM Solutions Group AG, Lübeck, Germany). The printer has build-volume of 125mm x 125mm x 12 mm and utilizes energy from single 400 W Ytterbium fiber laser. Gas atomized SS316L powder acquired from SLM solutions AG was used for printing. The chemical composition of the powder is listed in Table 3 and a representative scanning electron microscope (SEM) micrograph is shown in Figure 1.

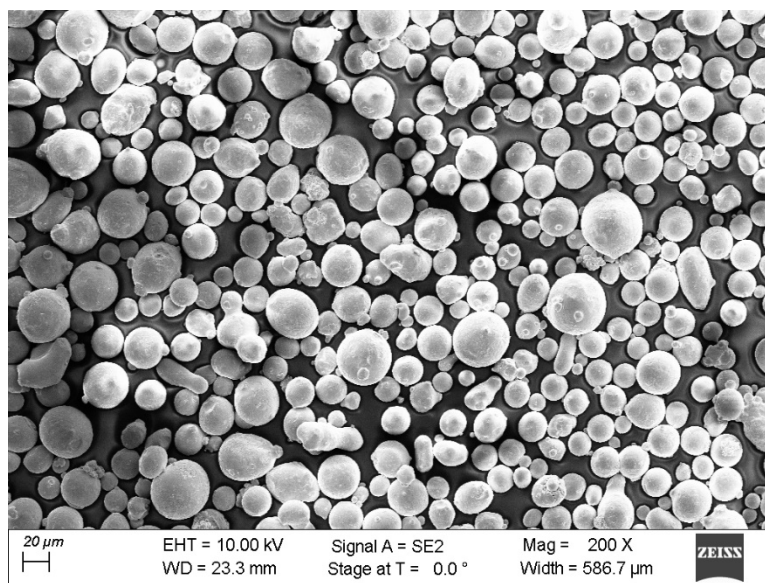


Figure 1. SEM image of fresh SS316L powder used for 3D printing.

Table 3: The chemical composition of SS316L powder obtained from SLM solutions

Element	Fe	Cr	Ni	Mo	Nb + Ta	Mn	Si	P	S	C	N	O
Mass fraction (%)	Balance	16-18	10-14	2-3	-	2	1	0.045	0.03	0.03	0.1	-

2.3 Experimental Procedure

The printed samples were separated from the build plate with the help of a wire electrical discharge machine (EDM). A Pace technology ALPHA MHT-1000Z Microhardness Tester (Pace Technologies, Tucson, AZ, U.S.A) was used to determine the Vickers microhardness of the samples. A total of 4 indentations were made on each sample along the build direction and the average values are reported. Each indentation was made with a load of 10 kg and was applied for 10 seconds based on ASTM E92 standard [24]. A Keyence VHX-970FN digital microscope (Keyence Corp of America, Itasca, IL, U.S.A) was used to determine the roughness of the side surface of the samples. The samples were placed on a sample holder and aligned on the edges in order to maintain the consistency in the roughness measurements. The controller is used to focus on the sample and three measurements for arithmetic mean roughness (Ra) were taken and the average values are reported.

3. Results and Discussion

3.1 Vickers Microhardness Analysis

The Vickers microhardness values were measured on the side surface for all the 32 as-built samples. The Vickers microhardness values, and the resulting contour plots along with the main effects plot are presented in Table 4 and Figure 2, respectively. As the scan strategy and scan speed are respectively changed from stripes to chess and 770 mm/s to 830 mm/s, with constant laser power of 185 W and hatch spacing of 117 μm , the hardness values increase from 241.27 HV to 266.24 HV. Similarly, when the scan strategy changed from stripes to chess and the hatch spacing increased from 111 μm to 129 μm , the hardness value increases from 242.74 HV to 258.90 HV for constant values of laser power (185 W) and scan speed (710 mm/s). It is observed that the scan strategy affects the hardness of the as-built samples the most. The increase in hardness value for chess scan strategy might be due to the difference in the microstructure to the corresponding samples. The similar effect was found by Rashid *et al.* [25]. The hardness values were found to decrease from 249.65 HV to 242.74 HV when the laser power increased from 150 W to 185 W for same values of scan speed (710 mm/s) and hatch spacing (111 μm) with the scan strategy (stripes) being the same for both the samples. Higher energy density values are found to promote epitaxial bonding and affects the chemical bonding of the tracks and layers. The hardness of is also affected by the microstructural defects such as pores and microcracks. Lower porosity leads to higher hardness values, which is an indication of proper interlayer binding and good adhesion between the layers. It is also noted that heat treatment enhances the hardness of the fabricated samples [21, 26].

Table 4: Average values of Vickers microhardness on the side surfaces of all samples

Sample No.	Scan Strategy	Laser Power (W)	Scan Speed (mm/s)	Hatch Spacing (μm)	Energy Density (J/mm^3)	Average Vickers Microhardness (HV)
1	Stripes	150	710	111	63.44	249.65 ± 2.75
2	Stripes	150	770	117	55.50	240.18 ± 6.36
3	Stripes	150	830	123	48.98	239.52 ± 4.45
4	Stripes	150	890	129	43.55	235.51 ± 4.96
5	Stripes	185	710	111	78.25	242.74 ± 2.01
6	Stripes	185	770	117	68.45	241.27 ± 4.94
7	Stripes	185	830	123	60.40	227.69 ± 6.98
8	Stripes	185	890	129	53.71	240.72 ± 5.95
9	Stripes	220	710	117	88.28	238.85 ± 8.38
10	Stripes	220	770	111	85.80	246.91 ± 3.91
11	Stripes	220	830	129	68.49	248.27 ± 6.27
12	Stripes	220	890	123	66.99	248.72 ± 5.52
13	Stripes	255	710	117	102.32	244.63 ± 5.08
14	Stripes	255	770	111	99.45	236.80 ± 1.63
15	Stripes	255	830	129	79.39	235.52 ± 5.72
16	Stripes	255	890	123	77.65	251.88 ± 3.99
17	Chess	150	710	129	54.59	257.12 ± 5.38
18	Chess	150	770	123	52.79	253.48 ± 2.55
19	Chess	150	830	117	51.49	245.71 ± 6.57
20	Chess	150	890	111	50.61	256.48 ± 8.50
21	Chess	185	710	129	67.33	258.90 ± 7.01
22	Chess	185	770	123	65.11	243.89 ± 6.10
23	Chess	185	830	117	63.50	266.24 ± 9.09
24	Chess	185	890	111	62.42	248.39 ± 3.70
25	Chess	220	710	123	83.97	250.59 ± 3.97
26	Chess	220	770	129	73.83	262.31 ± 9.07
27	Chess	220	830	111	79.60	258.25 ± 7.45
28	Chess	220	890	117	70.42	260.53 ± 6.82
29	Chess	255	710	123	97.33	234.29 ± 5.33
30	Chess	255	770	129	85.57	258.11 ± 7.13
31	Chess	255	830	111	92.26	251.40 ± 3.85
32	Chess	255	890	117	81.63	254.89 ± 5.87

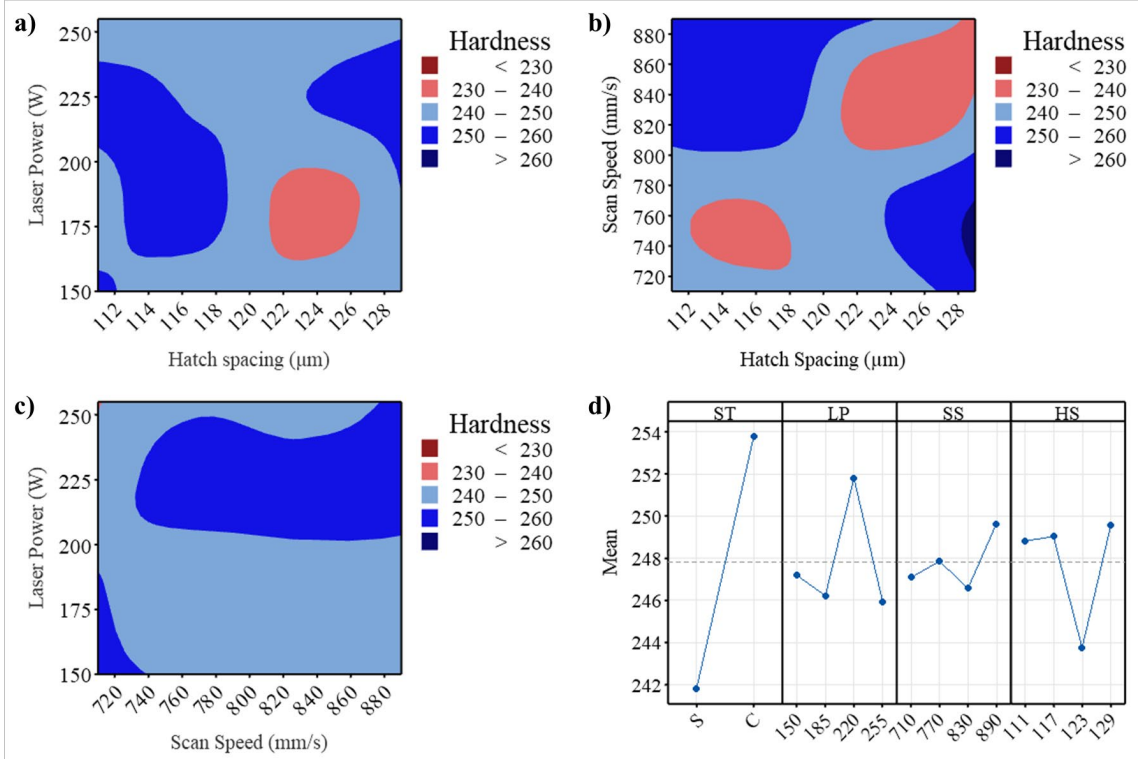


Figure 2. Contour plots showing the effect of a) laser power and hatch spacing b) scan speed and hatch spacing c) laser power and scan speed on microhardness d) Main effect analysis of microhardness.

3.2 Surface Roughness Analysis

The surface roughness analysis was carried out to evaluate the effect of process parameters on the surface finish of the as-built samples. The arithmetic mean roughness (R_a) values for the samples are listed in Table 5. The contour plots and the main effect analysis plot of the effect of different process parameter set is as shown in Figure 3. The surface roughness decreased (Table 5) with decreasing laser power when the scan strategy, hatch spacing, and scan speed were kept constant. At a constant hatch spacing of $129 \mu\text{m}$ and a scan speed of 830 mm/s and scan strategy of stripes, the surface roughness increases from $6.87 \mu\text{m}$ to $19.07 \mu\text{m}$ as the laser power increased from 220 W to 255 W . The roughness values drop from $4.4 \mu\text{m}$ to $2.06 \mu\text{m}$ as the scan speed is decreased from 830 mm/s to 770 mm/s with constant values of laser power (185 W) and hatch spacing ($123 \mu\text{m}$) and a change in scan strategy from stripes to chess. Finally, it was observed that the surface roughness decreases as the hatch spacing increases from $117 \mu\text{m}$ to $123 \mu\text{m}$ with constant laser power and scan speed values of 185 W and 770 mm/s . It was observed that laser power is most influential parameter affecting surface roughness compared to scan speed, hatch spacing and scan strategy. The high melt-pool temperatures are achieved due to higher values in laser power which in-turn results in material vaporization with recoil pressures [27]. Thus, an increase in the surface roughness of the samples is observed. A similar trend was observed by Leary *et al.* [27].

Table 5: Average values of Surface Roughness (R_a) on the top surfaces of all samples

Sample No.	Scan Strategy	Laser Power (W)	Scan Speed (mm/s)	Hatch Spacing (μm)	Energy Density (J/mm^3)	Surface Roughness R_a (μm)
1	Stripes	150	710	111	63.44	3.89 ± 1.42
2	Stripes	150	770	117	55.50	4.25 ± 0.52
3	Stripes	150	830	123	48.98	2.31 ± 0.20
4	Stripes	150	890	129	43.55	4.43 ± 0.59
5	Stripes	185	710	111	78.25	5.90 ± 1.53
6	Stripes	185	770	117	68.45	9.72 ± 3.64
7	Stripes	185	830	123	60.40	4.40 ± 1.67
8	Stripes	185	890	129	53.71	3.35 ± 0.39
9	Stripes	220	710	117	88.28	6.02 ± 1.97
10	Stripes	220	770	111	85.80	10.54 ± 2.62
11	Stripes	220	830	129	68.49	6.87 ± 2.21
12	Stripes	220	890	123	66.99	4.82 ± 2.35
13	Stripes	255	710	117	102.32	11.53 ± 3.63
14	Stripes	255	770	111	99.45	11.41 ± 2.43
15	Stripes	255	830	129	79.39	19.07 ± 2.53
16	Stripes	255	890	123	77.65	9.96 ± 1.52
17	Chess	150	710	129	54.59	3.51 ± 1.33
18	Chess	150	770	123	52.79	2.70 ± 0.23
19	Chess	150	830	117	51.49	2.40 ± 0.64
20	Chess	150	890	111	50.61	3.29 ± 0.90
21	Chess	185	710	129	67.33	4.06 ± 1.67
22	Chess	185	770	123	65.11	2.06 ± 0.45
23	Chess	185	830	117	63.50	5.53 ± 0.91
24	Chess	185	890	111	62.42	3.63 ± 0.40
25	Chess	220	710	123	83.97	9.66 ± 3.33
26	Chess	220	770	129	73.83	5.63 ± 0.80
27	Chess	220	830	111	79.60	5.58 ± 1.64
28	Chess	220	890	117	70.42	5.94 ± 1.60
29	Chess	255	710	123	97.33	14.40 ± 0.84
30	Chess	255	770	129	85.57	12.05 ± 2.43
31	Chess	255	830	111	92.26	5.50 ± 1.72
32	Chess	255	890	117	81.63	10.54 ± 1.91

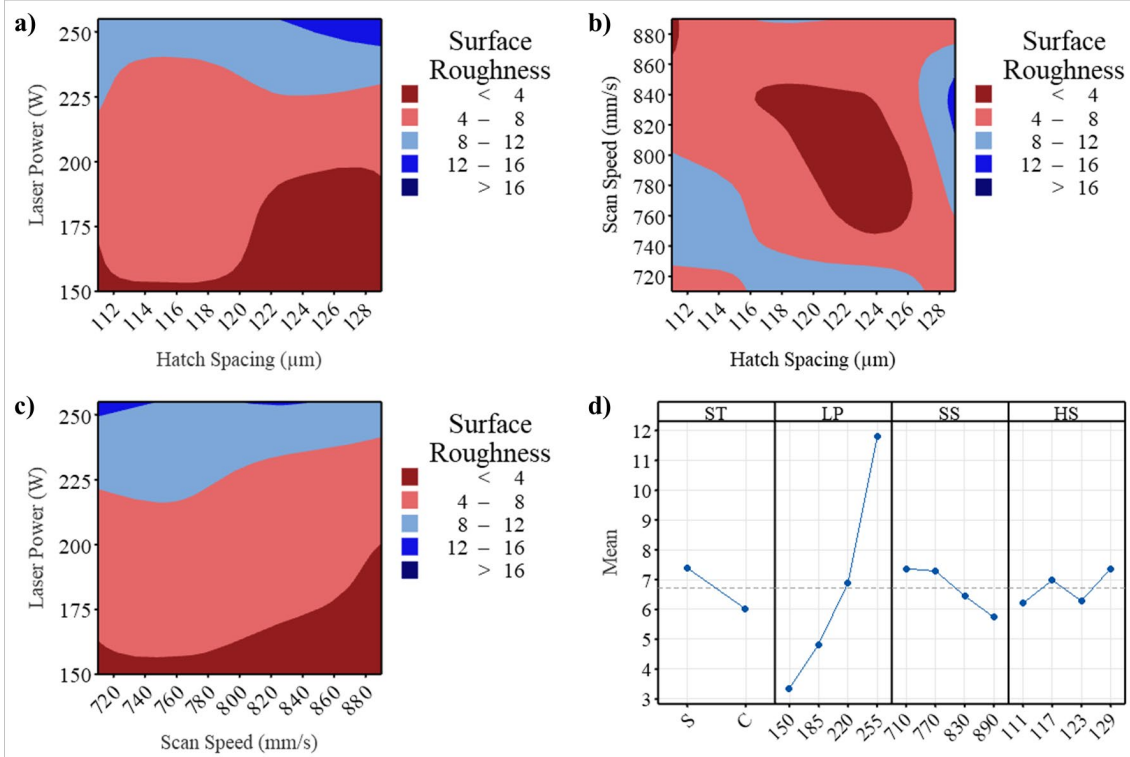


Figure 3. Contour plots showing effect of a) laser power and hatch spacing b) scan speed and hatch spacing c) laser power and scan speed on surface roughness d) Main effect analysis of surface roughness

4. Conclusion

In this work, the effect of process parameters on the properties of SS316L specimens are investigated with the help of Taguchi's mixed level design of experiments. Based on the principles of the Taguchi's methodology and the LPBF technique, it can be observed that the scan strategy plays a significant role in determining the microhardness values of the fabricated samples. Higher Vickers hardness values were obtained for the samples fabricated with chess scan strategy. The laser power was found to be the most influential parameter affecting the surface roughness values of the samples. The surface roughness was found to increase with an increase in the laser power of the samples.

5. Acknowledgement

This work was supported by a University of Texas System STARS award.

6. References

- [1] H. Gong, D. Snelling, K. Kardel, A. Carrano, Comparison of Stainless Steel 316L Parts Made by FDM- and SLM-Based Additive Manufacturing Processes, *JOM* 71(3) (2019) 880-885.
- [2] G. Sander, S. Thomas, V. Cruz, M. Jurg, N. Birbilis, X. Gao, M. Brameld, C.R. Hutchinson, On The Corrosion and Metastable Pitting Characteristics of 316L Stainless Steel Produced by Selective Laser Melting, *Journal of The Electrochemical Society* 164(6) (2017) C250-C257.
- [3] A.B. Kale, B.-K. Kim, D.-I. Kim, E.G. Castle, M. Reece, S.-H. Choi, An investigation of the corrosion behavior of 316L stainless steel fabricated by SLM and SPS techniques, *Materials Characterization* 163 (2020) 110204.
- [4] W. Fredriksson, D. Petrini, K. Edström, F. Björefors, L. Nyholm, Corrosion resistances and passivation of powder metallurgical and conventionally cast 316L and 2205 stainless steels, *Corrosion Science* 67 (2013) 268-280.
- [5] M. Fousova, D. Vojtech, J. Kubasek, D. Dvorsky, M. Machova, 3D Printing as an Alternative to Casting, Forging and Machining Technologies?, *Manufacturing Technology Journal* 15(5) (2015) 809-814.
- [6] B. Farhang, B.B. Ravichander, F. Venturi, A. Amerinatanzi, N. Shayesteh Moghaddam, Study on variations of microstructure and metallurgical properties in various heat-affected zones of SLM fabricated Nickel–Titanium alloy, *Materials Science and Engineering: A* 774 (2020) 138919.
- [7] R. Bharath Bhushan, Y. Zehao, K. Chen, M. Narges Shayesteh, A. Amirhesam, Development of ANN model for surface roughness prediction of parts produced by varying fabrication parameters, *Proc.SPIE*, 2021.
- [8] B. Farhang, B.B. Ravichander, J. Ma, A. Amerinatanzi, N. Shayesteh Moghaddam, The evolution of microstructure and composition homogeneity induced by borders in laser powder bed fused Inconel 718 parts, *Journal of Alloys and Compounds* 898 (2022) 162787.
- [9] B.B. Ravichander, K. Mamidi, V. Rajendran, B. Farhang, A. Ganesh-Ram, M. Hanumantha, N. Shayesteh Moghaddam, A. Amerinatanzi, Experimental investigation of laser scan strategy on the microstructure and properties of Inconel 718 parts fabricated by laser powder bed fusion, *Materials Characterization* 186 (2022) 111765.
- [10] B.B. Ravichander, S. Thakare, A. Ganesh-Ram, B. Farhang, M. Hanumantha, Y. Yang, N. Shayesteh Moghaddam, A. Amerinatanzi, Cost-Aware Design and Fabrication of New Support Structures in Laser Powder Bed Fusion: Microstructure and Metallurgical Properties, *Applied Sciences* 11(21) (2021).
- [11] S. Bahl, S. Mishra, K.U. Yazar, I.R. Kola, K. Chatterjee, S. Suwas, Non-equilibrium microstructure, crystallographic texture and morphological texture synergistically result in unusual mechanical properties of 3D printed 316L stainless steel, *Additive Manufacturing* 28 (2019) 65-77.
- [12] B.B. Ravichander, A. Rahimzadeh, B. Farhang, N. Shayesteh Moghaddam, A. Amerinatanzi, M. Mehrpouya, A Prediction Model for Additive Manufacturing of Inconel 718 Superalloy, *Applied Sciences* 11(17) (2021).
- [13] M. Ahmed Obeidi, S.M. Uí Mhurchadha, R. Raghavendra, A. Conway, C. Souto, D. Tormey, I.U. Ahad, D. Brabazon, Comparison of the porosity and mechanical performance of 316L stainless steel manufactured on different laser powder bed fusion metal additive manufacturing machines, *Journal of Materials Research and Technology* 13 (2021) 2361-2374.
- [14] W.M. Tucho, V.H. Lysne, H. Austbø, A. Sjolyst-Kverneland, V. Hansen, Investigation of effects of process parameters on microstructure and hardness of SLM manufactured SS316L, *Journal of Alloys and Compounds* 740 (2018) 910-925.

- [15] J.A. Cherry, H.M. Davies, S. Mehmood, N.P. Lavery, S.G.R. Brown, J. Sienz, Investigation into the effect of process parameters on microstructural and physical properties of 316L stainless steel parts by selective laser melting, *The International Journal of Advanced Manufacturing Technology* 76(5) (2015) 869-879.
- [16] A. Laohaprapanon, P. Jeamwattthanachai, M. Wongcumchang, N. Chantarapanich, S. Chantawerod, K. Sitthiseripratip, S. Wisutmethangoon, Optimal Scanning Condition of Selective Laser Melting Processing with Stainless Steel 316L Powder, *Advanced Materials Research* 341-342 (2012) 816-820.
- [17] D. Aqilah, M. Sayuti, F. Yusof, Y. Dambatta, N.A. Mohd Amran, W. Izzati, Effects of Process Parameters on the Surface Roughness of Stainless Steel 316L Parts Produced by Selective Laser Melting, *Journal of Testing and Evaluation* 46 (2018) 20170140.
- [18] T. Koziar, J. Bochnia, The Influence of Printing Orientation on Surface Texture Parameters in Powder Bed Fusion Technology with 316L Steel, *Micromachines* 11(7) (2020).
- [19] S. Greco, K. Gutzeit, H. Hotz, B. Kirsch, J.C. Aurich, Selective laser melting (SLM) of AISI 316L—impact of laser power, layer thickness, and hatch spacing on roughness, density, and microhardness at constant input energy density, *The International Journal of Advanced Manufacturing Technology* 108(5) (2020) 1551-1562.
- [20] A. Khorasani, I. Gibson, U.S. Awan, A. Ghaderi, The effect of SLM process parameters on density, hardness, tensile strength and surface quality of Ti-6Al-4V, *Additive Manufacturing* 25 (2019) 176-186.
- [21] B.B. Ravichander, A. Amerinatanzi, N. Shayesteh Moghaddam, Study on the Effect of Powder-Bed Fusion Process Parameters on the Quality of as-Built IN718 Parts Using Response Surface Methodology, *Metals* 10(9) (2020).
- [22] R. Bharath Bhushan, F. Behzad, S. Nahid, A. Amirhesam, M. Narges Shayesteh, Analysis of the deviation in properties of selective laser melted samples fabricated by varying process parameters, *Proc.SPIE*, 2020.
- [23] R. Bharath Bhushan, F. Carolina, A. Amirhesam, M. Narges Shayesteh, A framework for the optimization of powder-bed fusion process, *Proc.SPIE*, 2021.
- [24] A. International, Standard Test Methods for Vickers Hardness and Knoop Hardness of Metallic Materials, ASTM E92-17, ASTM International, 2017.
- [25] R. Rashid, S.H. Masood, D. Ruan, S. Palanisamy, R.A. Rahman Rashid, M. Brandt, Effect of scan strategy on density and metallurgical properties of 17-4PH parts printed by Selective Laser Melting (SLM), *Journal of Materials Processing Technology* 249 (2017) 502-511.
- [26] Z. Wang, K. Guan, M. Gao, X. Li, X. Chen, X. Zeng, The microstructure and mechanical properties of deposited-IN718 by selective laser melting, *Journal of Alloys and Compounds* 513 (2012) 518-523.
- [27] M. Leary, M. Khorasani, A. Sarker, J. Tran, K. Fox, D. Downing, A. Du Plessis, 7 - Surface roughness, in: I. Yadroitsev, I. Yadroitsava, A. du Plessis, E. MacDonald (Eds.), *Fundamentals of Laser Powder Bed Fusion of Metals*, Elsevier2021, pp. 179-213.